NaI gamma camera performance for high energies

Effects of crystal thickness, photomultiplier tube geometry and light guide thickness

Cosmi, Valerio; Wang, Beien; Goorden, Marlies C.; Beekman, Freek J.

DOI
10.1002/mp.17043

Publication date
2024

Document Version
Final published version

Published in
Medical Physics

Citation (APA)
Cosmi, V., Wang, B., Goorden, M. C., & Beekman, F. J. (2024). NaI gamma camera performance for high energies: Effects of crystal thickness, photomultiplier tube geometry and light guide thickness. *Medical Physics*, *51*(7), 4696-4708. https://doi.org/10.1002/mp.17043

Received: 28 June 2023 | Revised: 18 December 2023 | Accepted: 12 March 2024

DOI: 10.1002/mp.17043

RESEARCH ARTICLE

MEDICAL PHYSICS

NaI gamma camera performance for high energies: Effects of crystal thickness, photomultiplier tube geometry and light guide thickness

Valerio Cosmi[1] | **Beien Wang**[1] | **Marlies C. Goorden**[1] | **Freek J. Beekman**[1,2]

[1]Department of Radiation Science and Technology, Delft University of Technology, Delft, The Netherlands

[2]Free Bee International, Gouda, The Netherlands

Correspondence
Valerio Cosmi, Delft University of Technology, Mekelweg 15, 2629 JB Delft, The Netherlands.
Email: v.cosmi@tudelft.nl

Funding information
Dutch Research Council

Abstract

Background: Gamma camera imaging, including single photon emission computed tomography (SPECT), is crucial for research, diagnostics, and radionuclide therapy. Gamma cameras are predominantly based on arrays of photon multipliers tubes (PMTs) that read out NaI(Tl) scintillation crystals. In this way, standard gamma cameras can localize γ-rays with energies typically ranging from 30 to 360 keV. In the last decade, there has been an increasing interest towards gamma imaging outside this conventional clinical energy range, for example, for theragnostic applications and preclinical multi-isotope positron emission tomography (PET) and PET-SPECT. However, standard gamma cameras are typically equipped with 9.5 mm thick NaI(Tl) crystals which can result in limited sensitivity for these higher energies.

Purpose: Here we investigate to what extent thicker scintillators can improve the photopeak sensitivity for higher energy isotopes while attempting to maintain spatial resolution.

Methods: Using Monte Carlo simulations, we analyzed multiple PMT-based configurations of gamma detectors with monolithic NaI (Tl) crystals of 20 and 40 mm thickness. Optimized light guide thickness together with 2-inch round, 3-inch round, 60×60 mm^2 square, and 76×76 mm^2 square PMTs were tested. For each setup, we assessed photopeak sensitivity, energy resolution, spatial, and depth-of-interaction (DoI) resolution for conventional (140 keV) and high (511 keV) energy γ using a maximum-likelihood algorithm. These metrics were compared to those of a "standard" 9.5 mm-thick crystal detector with 3-inch round PMTs.

Results: Estimated photopeak sensitivities for 511 keV were 27% and 53% for 20 and 40 mm thick scintillators, which is respectively, 2.2 and 4.4 times higher than for 9.5 mm thickness. In most cases, energy resolution benefits from using square PMTs instead of round ones, regardless of their size. Lateral and DoI spatial resolution are best for smaller PMTs (2-inch round and 60×60 mm^2 square) which outperform the more cost-effective larger PMT setups (3-inch round and 76×76 mm^2 square), while PMT layout and shape have negligible ($< 10\%$) effect on resolution. Best spatial resolution was obtained with 60×60 mm^2 PMTs; for 140 keV, lateral resolution was 3.5 mm irrespective of scintillator thickness, improving to 2.8 and 2.9 mm for 511 keV with 20 and 40 mm thick crystals, respectively. Using the 3-inch round PMTs, lateral resolutions of 4.5

and 3.9 mm for 140 keV and of 3.5 and 3.7 mm for 511 keV were obtained with 20 and 40 mm thick crystals respectively, indicating a moderate performance degradation compared to the 3.5 and 2.9 mm resolution obtained by the standard detector for 140 and 511 keV. Additionally, DoI resolution for 511 keV was 7.0 and 5.6 mm with 20 and 40 mm crystals using 60 × 60 mm^2 square PMTs, while with 3-inch round PMTs 12.1 and 5.9 mm were obtained.

Conclusion: Depending on PMT size and shape, the use of thicker scintillator crystals can substantially improve detector sensitivity at high gamma energies, while spatial resolution is slightly improved or mildly degraded compared to standard crystals.

KEYWORDS
gamma camera, high energies, maximum-likelihood

1 | INTRODUCTION

Planar gamma cameras and single photon emission computed tomography (SPECT) are key for research, diagnostics, and radionuclide therapy.[1,2] Although solid state gamma cameras are gaining popularity, today's planar and SPECT imaging systems are still predominantly based on gamma detectors employing continuous NaI scintillation crystals coupled to an array of photomultiplier tubes (PMTs). These components, together with a collimator, define the basic structure of the so-called Anger camera, a nuclear-imaging instrument first developed in 1957.[3] More than seven decades later, this reliable camera technology is still very widely used as it grants an excellent balance between image quality and cost-effectiveness.[4]

Clinical gamma cameras typically operate within a γ energy range of 30–360 keV.[5] These cameras usually employ ∼ 9.5 mm thick NaI scintillation crystals which provide an excellent sensitivity, for example, ∼90% photopeak efficiency for ^{99m}Tc that emits 140 keV photons. Additionally, these detectors are characterized by a good energy resolution for the most often used isotopes (∼10% for ^{99m}Tc[6,7]) and a moderate intrinsic spatial resolution of ∼3.5 mm. The intrinsic resolution of a detector, together with the collimator's geometrical resolution, are among the main factors defining the whole system spatial resolution. In clinical SPECT, image resolution is usually 7−10 mm for general purpose systems and is mainly limited by the collimator. In preclinical SPECT instead, reconstructed image resolutions much better than the 3.5 mm intrinsic detector resolution are required. To achieve such high 3D image resolution, modern preclinical SPECT scanners often are equipped with multi-pinhole collimators. This gives the opportunity to exploit pinhole magnification, allowing these systems to attain a spatial resolution of 0.25 mm in vivo in mice,[6] which further improves to 0.12 mm[7] for ex vivo mouse organ imaging.

Interest in imaging isotopes with energies outside the conventional SPECT range is increasing as it can be valuable in multiple fields.[8,9] For instance, high energy γ imaging is important for cancer therapy with, for example, the combined γ—ß emitter ^{131}I (364 keV γ from its decay).[10] Interesting implementations also reside in cardiac imaging, where it was already demonstrated decades ago that injured but viable myocardium's regions can be evaluated with a SPECT camera using ^{99m}Tc-MIBI/^{18}FDG (requiring combined 140–511 keV γ imaging), improving patient convenience and cost-effectiveness.[11] New promising opportunities for high energy radionuclide therapy with α-particle emitters that also emit γ, such as ^{225}Ac and ^{213}Bi, are being investigated as well. Here, imaging of high-energy (440 keV from ^{213}Bi decay) γ is required for adequate biodistribution and dosimetry studies.[12] Additionally, in a recent preclinical study[13] it was shown that it is possible to image PET radioisotopes, such as ^{124}I and ^{89}Zr, without positron range blurring via their large amounts of high-energy prompt γ (603 and 909 keV γ respectively) emissions. This approach invalidates strong image blurring effects due to positron range while also enabling simultaneous imaging of multiple PET isotopes.

For the high energy isotopes mentioned above, the sensitivity of 9.5 mm thick NaI crystals is limited (e.g., ∼12% of 511 keV γ end up in the photopeak[14]). Therefore, it is highly important to improve detector sensitivity for high-energy γ-rays, particularly when spatial resolution can be preserved. Considering the significance of cost-effectiveness for SPECT, it is desirable that such an improvement in sensitivity would be achieved in a cost-effective and straightforward way. In that regard, a possible solution consists in increasing the scintillator's thickness. Research and development of gamma detectors already explored designs with thicker scintillation crystals than standard 9.5 mm in the late 90s (ADAC Forte, 16 mm thick crystal gamma detector). Today, numerous systems with thicker crystals are available on the market with applications in both the clinical (Siemens Pro.SPECT, 9.5 or 15.9 mm thick crystal; Mediso Anyscan Trio SPECT/CT, 9.5 or 15.9 mm thick

crystal) and preclinical (MILabs VECTor, 9.5 or 19 mm thick crystal) field of nuclear medicine.

The use of thicker crystals in these systems helped increase the sensitivity for high energy isotopes, but the possibility of further improving this result remains compelling. Therefore, it would be interesting to study even thicker crystals and evaluate their performance. However, further increasing the scintillator's thickness can negatively impact spatial resolution. This is due to the increased light spread within the crystal and the large variation in the depth-of-interaction (DoI) of the γ radiation.[15] Such DoI is not estimated in conventional gamma detectors which only provide a 2D interaction position. This may lead to parallax errors for scanner geometries where the γ enters the detector under an angle, for example, for diverging, converging or pinhole collimators. Different techniques have been studied to alleviate the DoI limitations affecting pinhole SPECT including software-based modeling and corrections, the use of curved fiber bundles to collimate light from a curved scintillator, and the application of a laser processed scintillator with converging pixels.[16–19] Another possible solution to mitigate this issue and preserve spatial resolution consists of estimating the 3D interaction position. This estimation would be useful for crystals thicker than what is currently available on the market, but it could also be beneficial for already existing gamma cameras.

An example high-energy preclinical SPECT system that could benefit from above-mentioned detector developments is VECTor (Versatile Emission Computed Tomography, MILabs B.V.[20]) that was partly developed in our group and that was used for several of the preclinical imaging studies with high-energy γ emitters described earlier (e.g.,[12,13]). VECTor uses high energy clustered multi-pinhole collimation[14,21] suitable for γ over a wide energy range (30–1000 keV). This system allows for sub-millimeter simultaneous PET-SPECT, sub-millimeter imaging of high-energy theragnostic isotopes and positron-range free and multi-isotope PET. VECTor is characterized by large-area PMT-based gamma detectors in a triangular set-up, meaning that the aforementioned DoI estimation is particularly relevant as γ can enter the detector under a large angle.

The goal of this work is to explore how much increasing the thickness of a scintillator would improve the photopeak sensitivity of a detector, while at the same time quantifying its effect on the detector's intrinsic spatial resolution. For this purpose, we conducted a Monte Carlo simulation study of multiple setups applying different NaI(Tl) scintillator thicknesses, several light guide thicknesses, and various PMT configurations. A maximum likelihood (ML) algorithm was used to estimate the 3D interaction position. This methodology was applied to γ of 140 and 511 keV, as these are the energies of frequently used SPECT radiotracers and of PET annihilation photons.

2 | MATERIALS AND METHODS

2.1 | Detector description

In the present extensive simulation study, we designed gamma detectors based upon the geometry of the ones used in VECTor systems. We compared detectors equipped with large-area 590 × 470 mm monolithic NaI(Tl) scintillation crystals, with thicknesses of 9.5, 20 and 40 mm. The 9.5 mm thick crystal was selected as a benchmark since it is widely used in conventional detectors. The 20 mm was chosen as it is comparable to the crystal thickness (19 mm) used by few systems available on the market. Finally, the 40 mm thick crystal was selected since it can greatly improve sensitivity for high energy γ compared to standard crystals.

In our simulation model built using GATE v9.0,[22] scintillators were assumed to be placed inside an aluminum frame. Their sides and entrance surface were coated with Teflon tape (Lambertian reflector) to maximize light collection. The surface of such tape was assumed to be optically polished, with surface roughness set to 0.1 as indicated by GATE documentation. Furthermore, the finishes ("*groundbackpainted*") of such tape were selected to reflect the presence of airgaps between the tape and the structure coated with it. A box-shaped light guide made of glass was placed in front of the scintillator to optimize light collection. Its height and length were adapted to the different configurations of PMTs used. We tested light guide thicknesses of 2, 6, and 10 mm to analyze how this parameter would affect detector's performance. Such light guide values were selected as the results of a preliminary study with a larger range indicated that the chosen interval would be sufficient to convey the system performance trend. Like the scintillator crystal, the sides of the light guide were wrapped in a polished Teflon tape and protected by an aluminum frame. The interface between the scintillator and the light guide was treated as a specular surface which was modeled to consist of small micro-facets. The orientation of these micro-facets is characterized by the parameter σ_α, standardly set to 1.2°, which defines the standard deviation of the Gaussian distribution of the orientations of the micro-facets around the average surface normal. Moreover, this interface was assumed to be without any optical couplant. This decision was based on the results of a preliminary study where the impact of the optical gel on the detector's performance was assessed. This was done by placing a thin (~0.4 mm) layer of Silicone Epoxy with refractive index (R_{index}) 1.5 between the scintillator and light guide, reproducing the characteristics of an actual detector system available in our lab which will be discussed later. Results with and without this optical couplant have shown a difference within the interval defined by the simulation uncertainty. This was thanks to the matching R_{index} of the couplant and the glass light guide which prevented additional refractions as photons

traverse these two media. Therefore, while desirable in practical use, optical gel was left out of the simulation model as it would significantly increase computational load without providing relevant benefits.

For the readout, we analyzed four different configurations of PMTs with different geometries and layout. The PMTs were assumed to be equipped with bialkali photocathodes and are based on existing models produced by Hamamatsu Photonics. The choice of the PMTs' sizes and placement was deeply influenced by the need to use large-area crystals and by the desire to build a cost-effective system. When selecting PMTs, we tried to avoid an excessive deterioration of the spatial resolution compared to what is achieved with a 9.5 mm thick scintillator. In that regard, it is worth remarking that decreasing the sizes of the PMTs while increasing their total number generally grants better performance in terms of spatial resolution, because it allows to sample the light distribution at higher spatial frequency, improving the detector's response to small variations in the interaction position of the incident radiation.[23–25] However, this improvement in spatial resolution comes at an overall dramatically increased cost due to the higher number of light sensors and corresponding electronic channels required to cover the same detector area. For these reasons, we decided to use PMTs of similar or slightly smaller size compared to the light sensors commonly used in clinical gamma cameras. This allowed us to study detectors with costs comparable to the ones currently available on the market, as this is often required for practical use.

The PMTs' placement was defined to guarantee coverage of the detector's central area, while their positioning at the edges was not optimized as in this study, we decided to not focus on edge effects. The four PMTs configurations tested are illustrated in Figure 1 and they consist of: Fourty-nine 3-inch (76.2 mm) diameter round PMTs combined with six 2-inch (50.8 mm) diameter round PMTs, which represents the standard configuration currently used for VECTor's detectors; one hundred eight 2-inch (50.8 mm) diameter round PMTs, ninety-nine 60×60 mm^2 (~2-inch) square PMTs, and sixty-three 76×76 mm^2 (~3-inch) square PMTs. For square PMTs, we tested two different layouts to evaluate their impact on the spatial resolution. In the first one, called "standard," the centers of PMTs belonging to different rows are aligned. In the second one, called "shifted," the centers of PMTs belonging to different rows are shifted by half the size of the PMT. For round PMTs, the light guide surface between the light sensors was assumed to be coated with an absorptive black painting according to the characteristics of the detector module used for validation that will be discussed later. Such coating was replicated in the simulation by counting only photons that ended within the surface covered by the PMTs when reaching the interface between the light guide and the PMTs.

In a cost analysis of the configurations presented, it is important to remark that the price of PMTs is approximately independent of their size. Since the variation of the number of light sensors is the main element differentiating the configurations tested, it was used as an indicator of the cost variation between the different setups.

2.2 | Simulation setup and data acquisition process

Monte Carlo (MC) simulations were executed using GATE v9.0[22] which is based on Geant4 version 10.05. To describe γ and optical photon behavior, we included the following GATE electromagnetic and optical physics processes: photoelectric effect, Compton scattering, Rayleigh scattering, electron ionization, Bremsstrahlung, scintillation, bulk absorption, and optical processes at boundaries (e.g., total internal reflection, refraction, or reflection) depending on the surface properties. Photon interactions with all the scintillator crystal surfaces were modeled using the GATE UNIFIED model.[26] In this model, the user must set four probabilities to control the reflectance due to the following kind of reflections: Specular lobe, Specular spike, Backscatter spike, and Lambertian. These probabilities were kept with the original values provided by the simulation model guide.

In our work, we simulated the detector response to a perfectly collimated line source of 70 or 86 mm length depending on whether the smaller PMTs (2-inch round and 60×60 mm^2 square) or the larger PMTs (3-inch round and 76×76 mm^2 square) configurations were under analysis. This line source was set to emit, based on the scintillator's thickness, 30 000 or 40 000 perpendicular monoenergetic γ-rays of 140 and 511 keV. These values were selected to grant at least 20 000 events within the photopeak window in each configuration tested. The line source was positioned, along both x and y axis, above the center of a PMT and near the PMT's edge by applying a 30 mm shift. These positions were chosen based upon the NEMA suggested procedure[27] to evaluate a gamma camera intrinsic spatial resolution and we denote them by "PMT center" and "PMT edge" respectively. The former location represents a low-spatial-resolution region, while in the latter position, high spatial resolution can be achieved.[28] Data from these line source simulations were used to estimate the 3D interaction positions of emitted γ via ML and to evaluate the detector's performance. We expect that the performance for sources placed above the PMT's center and the PMT's edge will describe the behavior over the entire detector's central area thanks to the geometrical symmetry of the PMT placement.

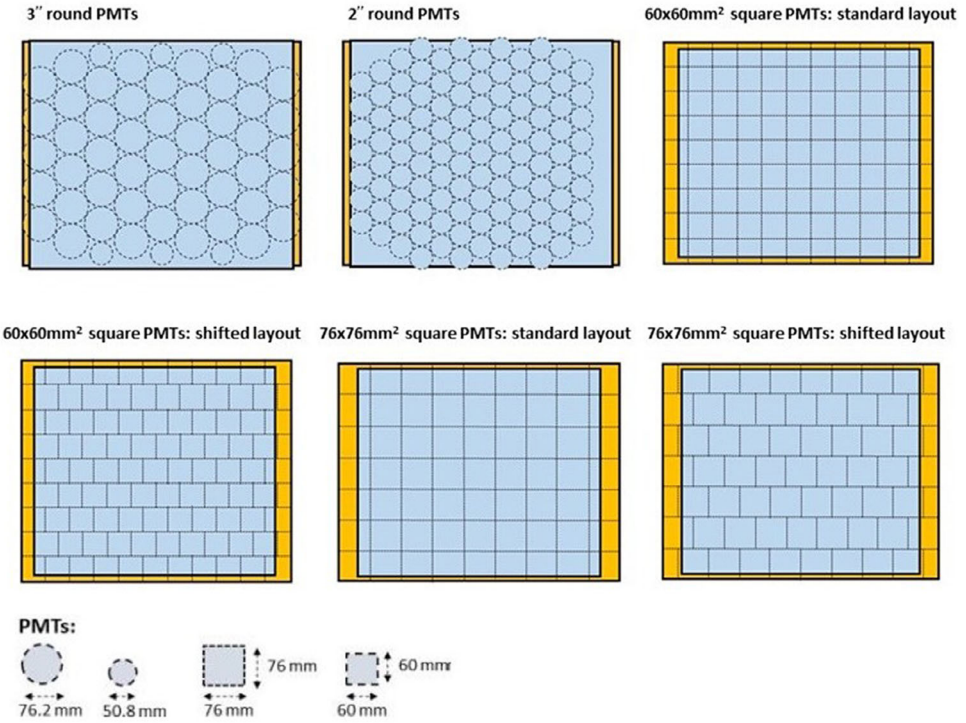

FIGURE 1 Schematic representation of the different PMT configurations studied. The yellow rectangle represents the light guide while the light blue indicates the scintillator. In each figure the outlines of the PMTs are shown to highlight the layout used. PMT, photomultiplier tube.

2.3 | Validation of simulation model

Prior to testing the thick scintillator designs we present, the simulation model was validated by comparing its results with experimental data previously collected.[29] Accordingly, we reproduced the same detector geometry consisting of a 9.5 mm thick crystal, a 16 mm thick light guide, and the 3-inch round PMT configuration described earlier. Such a setup was exclusively used for validation purposes. The data acquisition followed the same procedure as reported in the previous section.

For validation purposes, the detector performance was evaluated by using the same offline processing that was also applied to the experimental data,[29] consisting of a centroid estimation algorithm based on thresholding. The γ interaction positions were reconstructed via Anger Logic estimation, and the Line Response Functions (LRFs) were fitted with a Gaussian function. The full width at half maximum (FWHM) and full width at tenth maximum (FWTM) extracted from this fit were used to estimate the spatial resolution. This procedure was replicated for multiple sources within the 25–511 keV energy range.

2.4 | Maximum likelihood estimation and system matrix

While for validation purposes Anger logic was used, we intend to apply an ML algorithm to estimate the 3D interaction positions in the thicker scintillators. The ML algorithm takes advantage of the assumption that for γ photons with specified position of interaction and energy, the number of optical photons detected (n_m) by each PMT ($m = 0, 1, \ldots, M$) is Poisson distributed.[28] By calculating the mean value of such signal for every possible γ interaction location ($\bar{n}_m(x, y, z)$), we can define the log-likelihood that an interaction observed at the coordinate (x, y, z) results in output $\boldsymbol{n} = \{n_1, n_2, \ldots, n_M\}$ with the following equation, where constant terms were left out:

$$L(\boldsymbol{n}|x, y, z) = \sum_{m=0}^{M} \left\{ ln\left([\bar{n}_m(x, y, z)]^{n_m} \right) - \bar{n}_m(x, y, z) \right\}. \quad (1)$$

The γ interaction position ($\hat{x}, \hat{y}, \hat{z}$) that most likely generated $\boldsymbol{n}$ is obtained by maximizing (1). No accelerated search algorithm for the maximum was implemented as we utilized only a small portion of the detector's area.

To calculate $\bar{n}_m(x, y, z)$, we built a system matrix for each combination of PMT configuration and light guide thickness tested. This gave us the required information to relate the γ position of interaction to mean PMT signal. To generate these system matrices, a calibration measurement was simulated by placing the source at different positions in a grid configuration. The sizes of the grid were adjusted depending on the PMT setup under analysis: for the 2-inch round and 60 × 60 mm^2 square PMT configurations a 11 × 11 grid was used, whereas for the 3-inch round and 76 × 76 mm^2 square

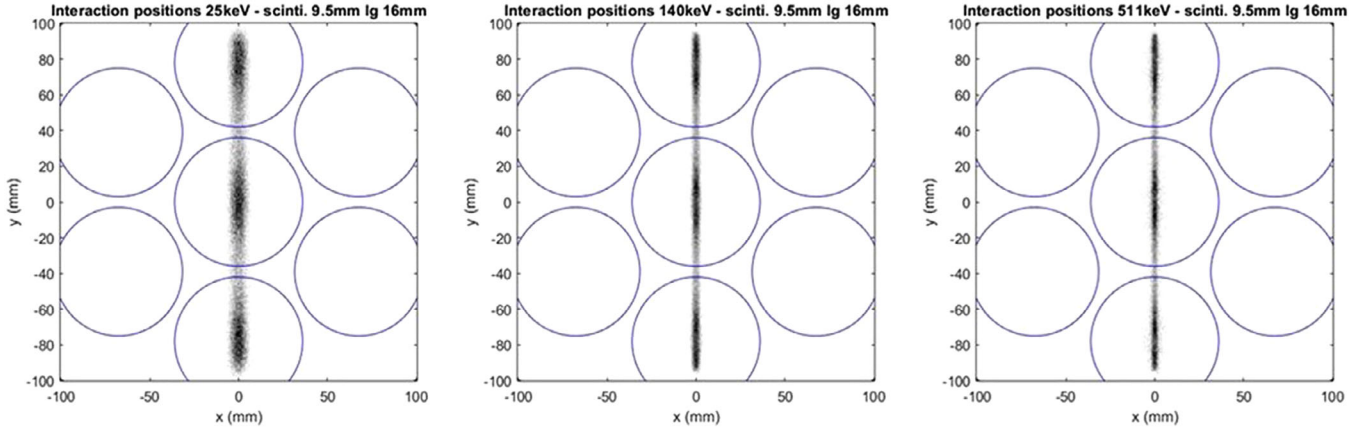

FIGURE 2 Line source images used for validation purposes. These images were acquired using a 9.5 mm thick scintillator (scinti.) and 16 mm thick light guide (lg) read out by the 3-inch round PMTs setup.[29] Equivalent images (not shown) were obtained with a horizontal line source. PMT, photomultiplier tube.

TABLE 1 Comparison of experimental and simulated spatial and energy resolution.

Source	Experimental FWHM [mm]	Experimental FWTM [mm]	Simulated FWHM [mm]	Simulated FWTM [mm]	Experimental E_{res} [%]	Simulated E_{res} [%]
^{125}I	7.1	13.4	7.0	13.1	22.7	22.5
^{99}Tc	3.6	7.0	3.5	6.3	10.0	9.8
^{22}Na	3.0	–	2.9	–	9.7	8.8

Note: Comparison of experimental and simulated spatial (FWHM and FWTM) and energy resolution (E_{res}) obtained for different sources.
Abbreviations: FWHM, full width at half maximum; FWTM, full width at tenth maximum.

PMT configurations the grid was 13 × 13. In both grids each node is 8 mm away from the adjacent ones. To produce almost noiseless system matrices, the total number of emissions simulated was such that a total of 121 000 (11 × 11 matrix) or 169 000 (13 × 13 matrix) γ were counted within the photopeak window, 1000 γ for each position. From each scintillation event generated by these γ, we extracted its signal distribution, consisting of M PMT outputs, where M refers to the total number of PMTs used. To improve the system matrix accuracy, we post-processed the simulated signals. We started by rejecting events resulting from large-angle Compton scatter using a preliminary Anger Logic position estimation. To this end, the 2D distribution of the coordinates estimated via Anger Logic was fitted with a 2D Gaussian and the FWHM along x and y axis was extracted. These FWHMs were then used to discard all events outside $0.9 \cdot FWHM$ along both axes. The described filtering process was applied to all grid positions, rejecting ∼38% and ∼32% of events respectively when working with 20 and 40 mm thick scintillators. Additionally, we identified and discarded PMTs that carried non-useful information. To do that, we calculated the mean PMT signals across all events generated from a specific grid position and compared it to a threshold value. This threshold was set to 1% of the sum of all PMT mean signals for the same grid position. As a result of the filtering process, we obtained for each event M'-dimensional data, with $M' < M$, containing information about the number of useful PMTs and the signal they detected.

In this simulation study, we decided to assess DoI in a realistic way as its ground truth value would not be known in an experimental calibration. To achieve that, we used the events' signal distribution and extracted the DoI information by applying a Factor Analysis (FA) statistical method to the filtered M'-dimensional data. Via the FA, we exploited the correlation between the DoI of an event and the width of its light distribution. In the FA algorithm, we decided to set the dimensionality of the latent space responsible for the variability among the correlated M'-dimensional simulation data to one. The obtained one-dimensional latent variable approximately indicates the DoI of each scintillation event analyzed. We then divided the scintillator into sections of 2 mm thickness and used the DoI estimated via FA to sort events in ascending DoI order. Each event was then placed accordingly into the corresponding section. Thanks to this process, we were able to model the mean detector response for scintillation events that happened at different depths within the scintillator crystal. This response was calculated for the events generated by placing the source in all the defined grid positions.

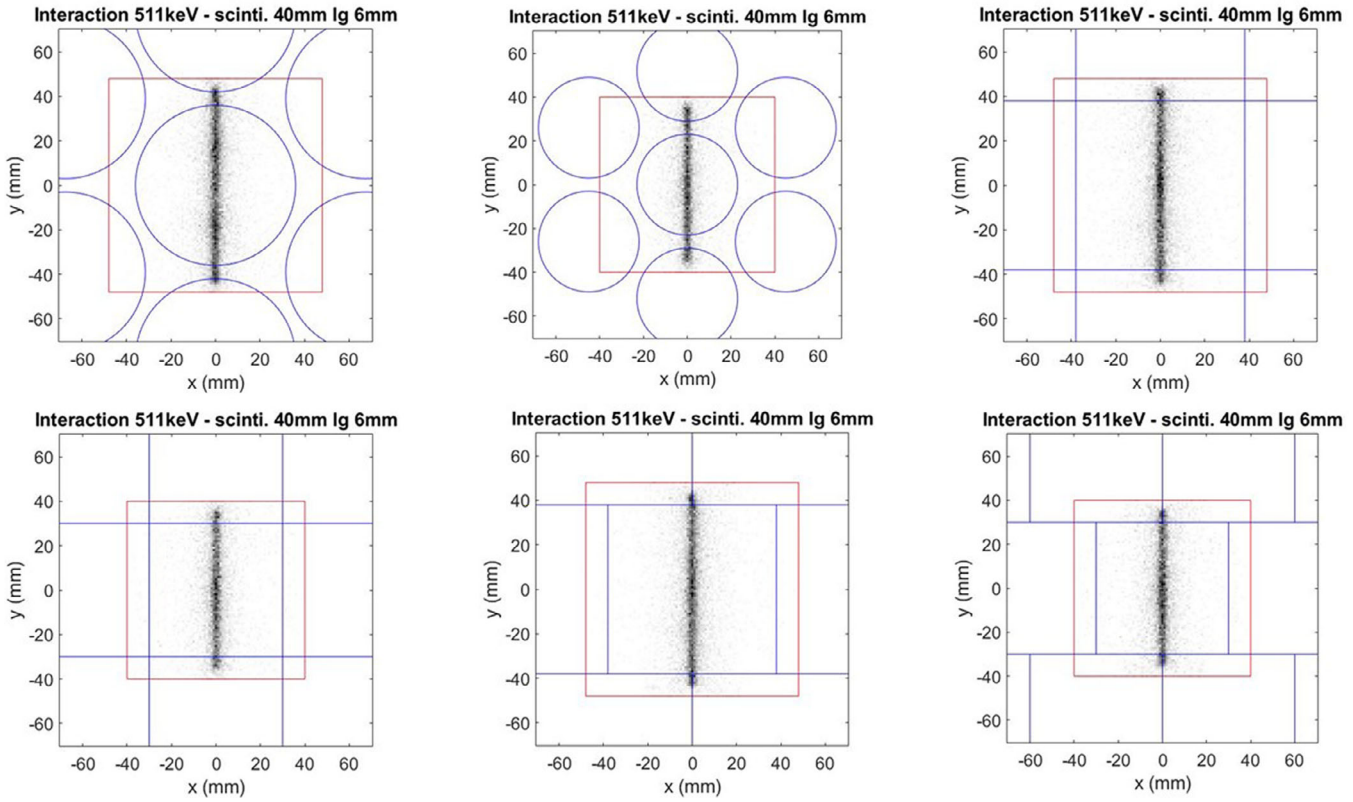

FIGURE 3 Line source images for a selected number of detector geometries. These images were acquired using a 40 mm thick scintillator (scinti.) and 6 mm thick light guide (lg) for all considered PMTs setup. These images were produced by placing the source at (0,0) mm, at the center of the PMT's photocathode area. PMT, photomultiplier tube.

The obtained mean values were used to build a preliminary 11 × 11x*S* system matrix with voxel size of 8 × 8 × 2 mm^3, where *S* refers to the number of sections in which the scintillator was divided. We further improved our matrix by interpolating the detector's response at intermediate steps using a smooth bivariate spline approximation, achieving a final 121 × 121x*S* system matrix with voxel size of 1 × 1 × 2 mm^3.

2.5 | Data analysis

Data acquired from system matrix and line source simulations were used in a MATLAB script to evaluate the detector's performance. To calculate energy resolution (E_{res}), we used the system matrix data as they are generated by irradiating the central part of the detector. This allowed us to evaluate the detector's mean response in that area which was then used to calculate the distribution of the sum of PMTs' outputs. The E_{res} was defined as the FWHM of this distribution as indicated by NEMA.[27]

To estimate the detector's lateral resolution, we first determined the 3D coordinates for each detected event. These coordinates were calculated by feeding energy filtered data into the ML algorithm to partially reject scatter events as it would be done in an experimental environment. The energy filtering consisted in applying an acceptance energy window of 20% and 15% respectively around the detected photopeak of 140 and 511 keV. From the algorithm's output we generated the *XY* planar distribution of the estimated positions of interactions and we projected these on either the x or y axis. Both projections were fitted with a two-term univariate Gaussian to extract their parameters, as a simple univariate Gaussian wasn't capable to accurately fit them. The resulting FWHMs were used to calculate the lateral resolution, defined as the Root Mean Square (RMS) average of the x and y projections' FWHM.

To determine the DoI resolution, first we compared the estimated DoI values to the ground truth values extracted from the simulation model. From these graphs, we extracted profiles at a simulated depth of 10 mm and fitted them with a three-term univariate Gaussian. The FWHMs extracted from these fits were then used to determine the DoI resolution. This resolution was only estimated for 511 keV data as for 140 keV γ interactions happen mostly at the top of the crystal and DoI information is not useful.

For both DoI and lateral resolution, uncertainty associated with the estimated values was calculated using the Root Mean Square Error (RMSE).

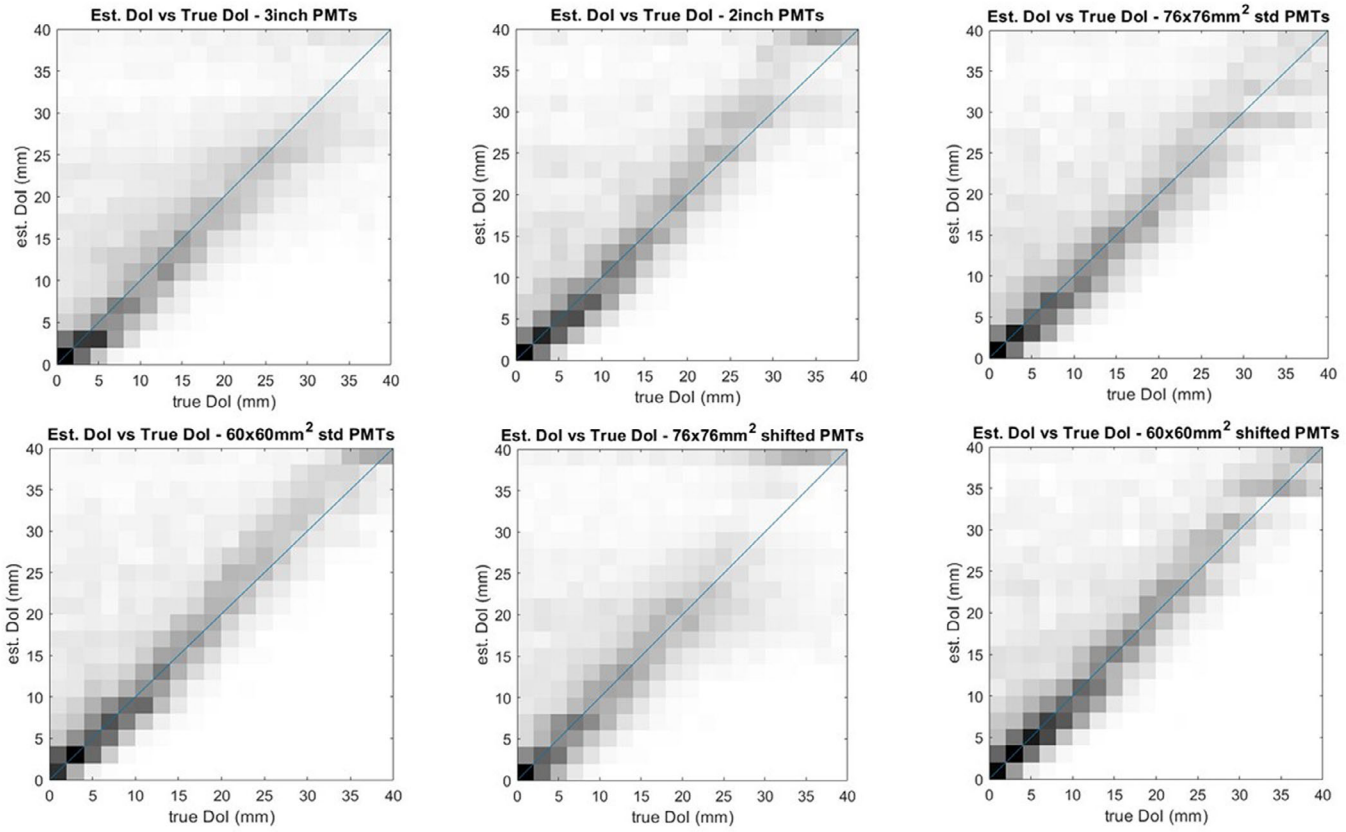

FIGURE 4 Comparison of estimated (Est.) versus true DoI for multiple detector geometries consisting of a 40 mm thick scintillator with 6 mm thick light guide for all considered PMTs setups. DoI, depth-of-interaction; PMT, photomultiplier tube.

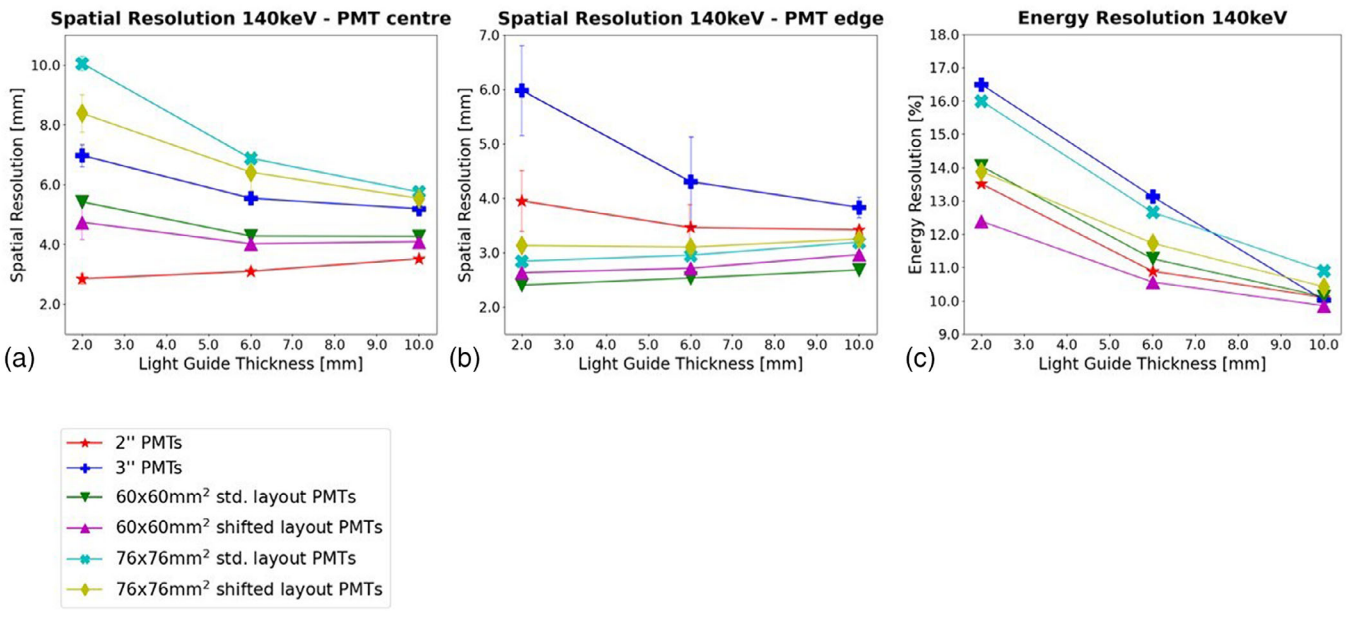

FIGURE 5 Comparison of spatial and energy resolution for all configurations with 20 mm thick crystal irradiated by 140 keV γ; PMT center (a) and PMT edge (b) results are presented in a separate set of graphs. To limit overlap the placement of error bars in the graphs was slightly shifted. PMT, photomultiplier tube.

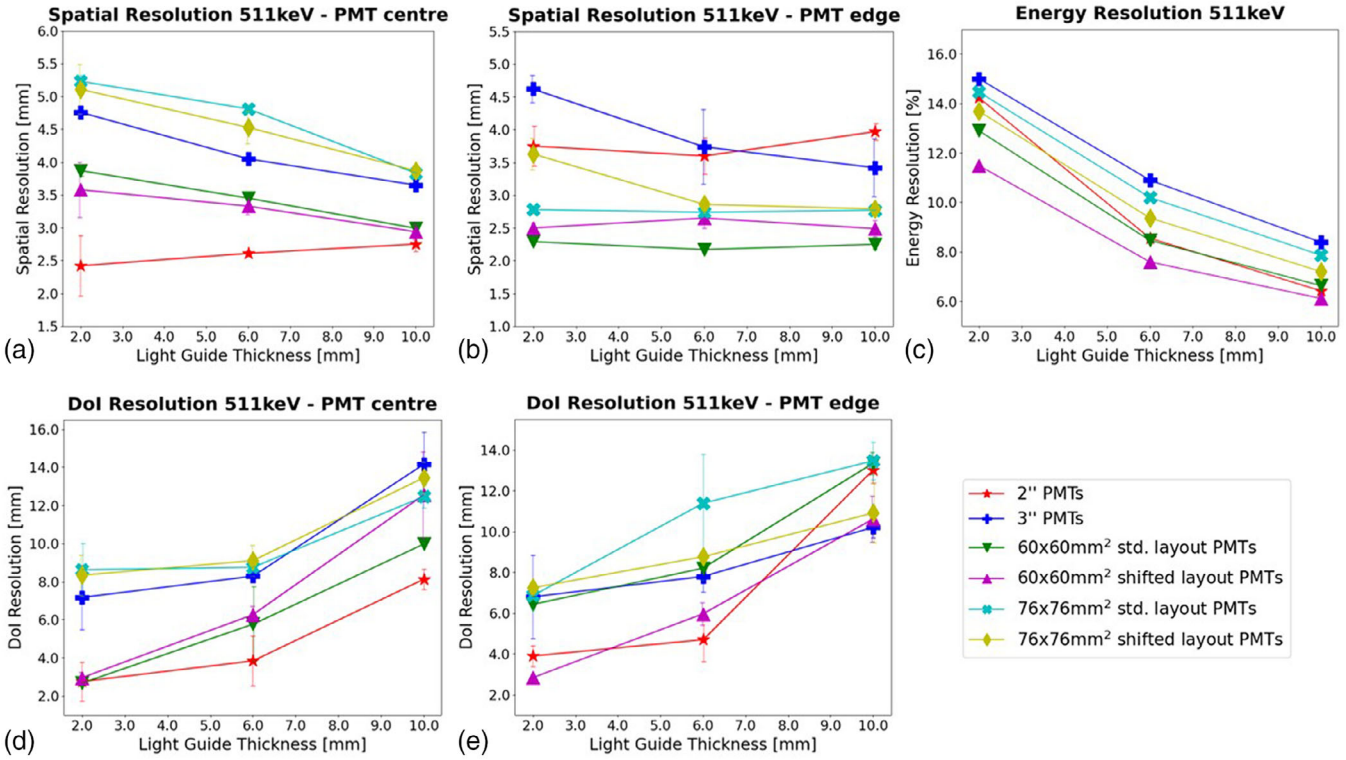

FIGURE 6 Comparison of spatial, DoI and energy resolution for all configurations with 20 mm thick crystal irradiated by 511 keV γ; PMT center (a, d) and PMT edge (b, e) results are presented in a separate set of graphs. To limit overlap the placement of error bars in the graphs was slightly shifted. DoI, depth-of-interaction; PMT, photomultiplier tube.

To calculate the photopeak sensitivity, the same energy acceptance windows defined for filtering the input ML data were used. The photopeak sensitivity was then calculated as the ratio of the γ that fell within these windows and the total number of emitted γ.

3 | RESULTS

The validation study confirmed the accuracy of the simulation model as we compared the measured and simulated FWHM, FWTM, and E_{res} at 25, 140, and 511 keV γ energy. Results for the 9.5 mm scintillator (scinti.) and 16 mm light guide (lg) are shown in Figure 2 and Table 1.

For the FWTM, experimental data for 511 keV is not available due to the strong background present in the images produced, therefore a comparison was not possible. Figure 3 illustrates the detector performance for the 511 keV line source for a few configurations. In these examples, we show results for the 40 mm scintillator equipped with a 6 mm light guide readout for all tested PMT setups. Figure 4 shows estimated DoI versus true DoI for the same setups as in Figure 3. Figures 5 and 6 provide an overview of E_{res}, lateral resolution as well as DoI resolution for all configurations with 20 mm thick crystals for 140 and 511 keV γ respectively. In Figures 7 and 8, the same performance metrics shown for the 20 mm thick scintillator in Figures 5 and 6 are presented for the 40 mm thick crystal when it is irradiated by 140 and 511 keV γ respectively.

TABLE 2 Performance obtained analyzing 140 keV γ with different scintillator's crystal thickness read out by 3-inch round PMTs.

Scintillator's thickness [mm]	E_{res} @ 140 keV	Lateral resolution @ 140 keV [mm]	Photopeak sensitivity
9.5	9.8%	3.5 ± 0.1	~88%
20	10.0%	4.5 ± 0.1	~97%
40	10.2%	3.9 ± 0.1	~97%

Note: Energy resolution, lateral resolution and photopeak sensitivity for 9., 20 and 40 mm thick crystal detector for 140 keV γ obtained with 3-inch round PMTs.
Abbreviation: PMT, photomultiplier tube.

In Tables 2 and 3, we compare the performance of systems with 20 and 40 mm thick crystals to that of a standard detector with a 9.5 mm thick crystal. These results were calculated by averaging the performance both at the center and at the edge of the PMT. The reported simulated results for 140 and 511 keV γ were obtained using the 3-inch round PMTs combined with the light guide which granted the best performance.

A further improvement of lateral and DoI resolution results compared to what can be obtained with

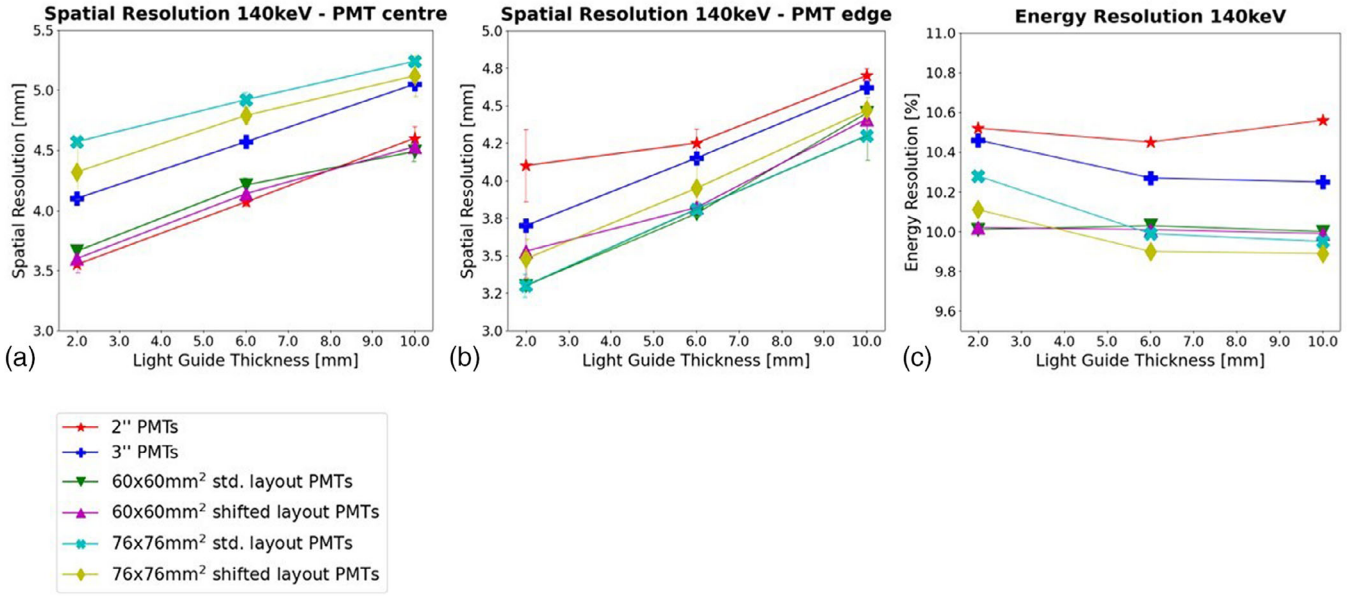

FIGURE 7 Comparison of spatial and energy resolution for all configurations with 40 mm thick crystal irradiated by 140 keV energy γ; PMT center (a) and PMT edge (b) results are presented in a separate set of graphs. To limit overlap the placement of error bars in the graphs was slightly shifted. PMT, photomultiplier tube.

TABLE 3 Performance obtained analyzing 511 keV γ with different scintillator's crystal thickness read out by 3-inch round PMTs.

Scintillator's thickness [mm]	E_{res} @ 511 keV	Lateral resolution @ 511 keV [mm]	DoI resolution @ 10 mm depth [mm]	Photopeak sensitivity
9.5	8.8%	2.9 ± 0.2	N.A.	~12%
20	8.2%	3.5 ± 0.2	12.1 ± 0.9	~27%
40	6.4%	3.7 ± 0.1	5.9 ± 0.2	~53%

Note: Energy resolution, lateral resolution, DoI resolution and photopeak sensitivity for 9.5, 20, and 40 mm thick crystal detector for 511 keV γ obtained with 3-inch round PMTs.
Abbreviation: PMT, photomultiplier tube.

TABLE 4 Spatial performance obtained for thick scintillator's crystal read out by 60 × 60 mm² square PMTs.

Scintillator's thickness [mm]	Lateral resolution @ 140 keV [mm]	Lateral resolution @ 511 keV [mm]	DoI resolution @ 10 mm depth [mm]
20	3.5 ± 0.3	2.8 ± 0.1	7.0 ± 1.0
40	3.5 ± 0.1	2.9 ± 0.1	5.6 ± 0.4

Note: Best lateral and DoI resolution for 20 and 40 mm thick crystal detector obtained with 60 × 60 mm² square PMTs.
Abbreviations: DoI, depth-of-interaction; PMT, photomultiplier tube.

3-inch round PMTs is possible when using one of the smaller PMTs configurations tested, as can be seen in Figures. 5,6,7, and 8. In Table 4, the best results obtained with 60 × 60 mm² square PMTs are provided, calculated as the mean between PMT center and PMT edge performance:

4 | DISCUSSION

We presented the results of an MC simulation study in which we investigated to what extent a photopeak sensitivity improvement of a PMT-based NaI(Tl) gamma detector for high energy γ would be possible, without seriously deteriorating its intrinsic spatial resolution. To this end, we studied gamma detectors with increased scintillator thicknesses for a series of light guide thicknesses read out by various PMT configurations. To mitigate a possible reduction in performance due to the increased scintillator thickness, we estimated the 3D interaction position of each event using an ML algorithm. The obtained DoI information is not available in standard gamma detectors. The performance for γ with energies of 140 and 511 keV was analyzed, and the results are presented in Tables 2, 3, and 4. The obtained values show that it is possible to significantly improve photopeak sensitivity by increasing the scintillator's thickness while using the same PMT configuration. Depending on PMT size, this improvement comes with only a modest degradation or a slight improvement of the intrinsic detector resolution.

For both detector designs with thicker scintillators, intrinsic spatial performance depends on PMT configuration as well as source location and light guide thickness. In general, PMT layout and shape have a negligible effect (< 10%) on spatial performance. Setups with smaller PMTs (2-inch round or 60 × 60 mm² square) perform best in terms of spatial and DoI resolution as can be seen from Figures 5, 6, 7, and 8. However, the cost of these configurations is significantly higher than of the ones equipped with larger PMTs (3-inch round

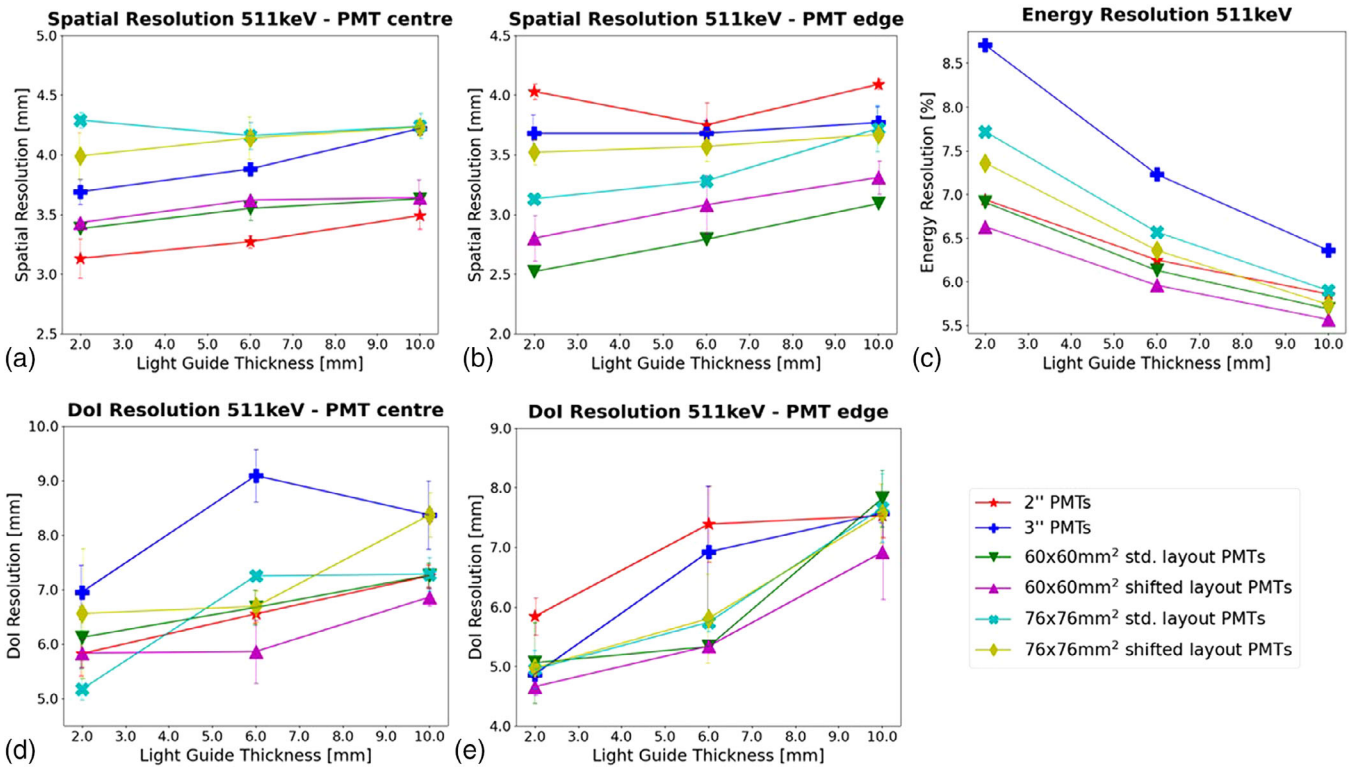

FIGURE 8 Comparison of spatial, DoI and energy resolution for all configurations with 40 mm thick crystal irradiated by 511 keV γ; PMT center (a, d) and PMT edge (b, e) results are presented in a separate set of graphs. To limit overlap the placement of error bars in the graphs was slightly shifted. DoI, depth-of-interaction; PMT, photomultiplier tube.

or 76 × 76 mm^2 square) due to the higher number of light sensors and electronic channels used. Making the rough assumption that costs scale linearly with number of required PMTs and channels, we estimate that compared to the current 3-inch round PMT configuration, the overall cost would increase by roughly ∼15% if 76 × 76 mm^2 square PMTs were utilized, whereas if the 60 × 60 mm^2 square or the 2-inch round configurations were to be used, the respective increments would be ∼80% or ∼97%. Regarding the source position, for a source placed above the PMT center, round PMTs grant better spatial and DoI resolution than square PMTs. Moving towards locations above the PMTs' edges instead, square PMTs allow to gain a moderate performance improvement. Concerning the influence of light guide thickness on the spatial performance, the 20 mm and the 40 mm thick crystal show different behaviors. The performance of the 20 mm scintillator for most configurations tends to slightly improve as the light guide thickness increases. This is probably because, due to their size, the PMTs used require larger light spread to grant optimal performance. However, excessively increasing the light guide thickness would lead to unwanted spreading of the signal between different light sensors, with a low number of events in each of them and hence performance degradation. These considerations together with the results shown in Figures 5 and 6 seem to suggest the existence of an optimal light guide thickness range for this crystal of around 10 mm. On the other hand, majority of 40 mm scintillator setups suffer from performance degradation when utilizing thicker light guides. This is probably due to the overall larger light spread of optical photons in a thicker crystal. It is important to remark that the improvement in spatial resolution observed for some configurations when increasing the light guide thickness is always compensated by a substantial degradation of the DoI resolution. Therefore, we believe that the overall spatial performance doesn't benefit from using thicker light guides.

Analyzing the 40 mm thick scintillator, the best results at the PMT center were achieved by the configuration with 2 mm light guide read out by 2-inch round PMTs. This setup obtained 3.5 mm spatial resolution for 140 keV photons (Figure 7a), while for 511 keV, it achieved 3.1 mm spatial resolution and 5.8 mm DoI resolution (Figure 8a,d). Near the PMTs' edges, the best spatial performance was reached by the setup equipped with 60 × 60 mm^2 square PMTs (std layout) and 2 mm light guide. This configuration achieved 3.3 mm spatial resolution for 140 keV (Figure 7b), while for 511 keV γ, the estimated spatial and DoI resolution were respectively 2.5 and 5.1 mm (Figures 8b,e). Regarding the average spatial performance over the analyzed detector's central area, the best results for the 40 mm thick

scintillator were reached using the 60 × 60 mm^2 square PMTs (std layout) combined with 2 mm light guide. This configuration obtained a spatial resolution of 3.5 mm for 140 keV, whereas for 511 keV, results were 2.9 and 5.6 mm, respectively, for spatial and DoI resolution.

When discussing DoI results, it is important to emphasize that high DoI resolution is not necessarily required for our thick detectors' designs. For example, the VECTor system partly developed in our group can attain up to 0.6 mm resolution ^{18}F-PET using 9.5 mm thick crystal detectors without any DoI estimation. Such a system is characterized by a DoI uncertainty equal to the scintillator thickness, and we used that as a reference value. In most of the configurations tested, except the ones consisting of 20 mm thick crystal with 10 mm light guide, the estimated DoI resolution was below this 10 mm threshold. This represents an acceptable value as it would guarantee to be in a situation comparable to what conventional detectors have at best.

In terms of E_{res}, results for thick and conventional crystal detectors are comparable when working with 140 keV γ, while for 511 keV γ, thick crystals allow to achieve improved E_{res}. These improvements could be related to the increased chance that γ that Compton scatter in their first interaction in the detector do not escape the scintillator but lose all their energy in subsequent interactions. An additional element that has an influence on the E_{res} is the shape of the PMTs used. Setups with square PMTs grant better performance compared to configurations with round PMTs. This is thanks to the increased percentage of the light sensors' active area covering the detector's surface, which improves detection of optical photons. Regarding the impact of the light guide thickness on this metric, both thicker crystals seem to benefit from the use of thicker light guides. This is likely because part of the points source locations is directly above the dead area of a PMT. In this case, working with thicker light guides increases the spread of optical photons, resulting in a higher probability of reaching the active area of a nearby PMT. However, such a trend won't extend indefinitely as with further increasing light spread optical photons will eventually reach the next dead area between PMTs. Moreover, as mentioned for the spatial performance, improvements in E_{res} achieved by further increasing the light guide thickness would be at the cost of the DoI resolution. Analyzing the 40 mm thick crystal, the best results were obtained using the 3-inch square PMTs (std layout) setup with a 10 mm light guide. This configuration reached an average E_{res} of 9.6% and 5.9%, respectively, for 140 keV (Figure 7c) and 511 keV γ (Figure 8c). On the other hand, the configuration consisting of 3-inch round PMTs combined with 10 mm light guide attained an average E_{res} of 9.9% for 140 keV γ (Figure 7c) and of 6.3% for 511 keV γ (Figure 8c).

Regarding the detector sensitivity, increasing the scintillator's thickness to 20 or 40 mm results in photopeak sensitivities respectively of ∼27% or ∼53% for 511 keV γ. These values are 2.2 and 4.4 times better than what can be obtained with a standard 9.5 mm thick scintillator. Such a high improvement in sensitivity comes at modest deterioration in spatial resolution when using a cost-effective PMT setup, as shown in Tables 2 and 3. However, by choosing a different PMT configuration (e.g., 2-inch round or 60 × 60 mm^2 square) it is possible to maintain the same high sensitivity while also improving the spatial performance as indicated in Table 4.

By analyzing the presented results, it is clear that in terms of spatial and DoI resolution, it would be highly beneficial to use smaller sized round or square PMTs. However, their overall higher cost is a relevant drawback in our study, as one of the goals of our work is to build a large-area cost-effective detector. Therefore, it is crucial to find the right balance between performance and cost. In this context, the 3-inch square PMTs could represent a valid option, as they offer moderately improved performance compared to the 3-inch round PMTs at a slightly higher cost.

A limitation of the present work is that a detailed performance analysis was executed for the central detector area while edge effects were not yet studied. Generally, the severeness of edge effects depends on crystal thickness and is therefore important when considering thick crystal detectors. However, for the large-area gamma detectors considered (590 × 470 mm^2), such dead edge effects are of lesser concern than when small crystals are used. Typically, for these large detectors, a rather substantial area near the crystal edge is simply not used (∼4.5 cm), a choice that can be made because this edge region is still relatively small compared to the whole crystal. Therefore, it is not expected that edge effects have a major influence within the FOV that is used in practice. To illustrate this, we conducted a small simulation study comparing the 9.5 and 40 mm thick crystals with the standard 3-inch PMT configuration (see Figure S1). The data reported in Table S1 indicates that for a 40 mm thick crystal, spatial resolution near the edge only deteriorates moderately (< 15%) while it remains constant for the 9.5 mm crystal. Although the illustrated results don't represent an in-depth analysis of the relation between crystal thickness and the extent of edge effects, they indicate that even for the worst-case scenario (thickest crystal and largest PMTs) edge effects are not severely influencing the overall detector performance.

5 | CONCLUSION

We explored a possible cost-effective solution to improve sensitivity for high-energy γ outside the conventional SPECT energy range. We have shown that increasing the scintillator's thickness can greatly

improve the detector photopeak sensitivity for high-energy γ. Moreover, we illustrated how the spatial resolution can be influenced by changes in light guide thickness and PMT geometry. Depending on PMT geometry, and thus on cost-effectiveness, spatial resolution of gamma detectors with thick scintillators can be slightly improved or moderately degraded compared to conventional gamma detectors.

ACKNOWLEDGMENTS

This work was financed by the research grant QUARAT: Quantitative Universal Radiotracer Tomography (TTW16885) which is financed in part by the Dutch Research Council (NWO).

CONFLICT OF INTEREST STATEMENT

The authors declare no conflicts of interest to disclose.

REFERENCES

1. Cherry SR. *Physics in Nuclear Medicine*. Elsevier Inc; 2012.
2. Weissleder R. *Molecular Imaging: Principles and Practice*. People's Medical Publishing House; 2010.
3. Anger HO. *The Scintillation Camera : A New Instrument for Mapping the Distribution of Radioactive Isotopes*. University of California Radiation Laboratory; 1957.
4. Peterson TE, Furenlid LR. SPECT detectors: the Anger Camera and beyond. *Phys Med Biol*. 2011;56(17):R145-R182.
5. Chen Y. *Image Acquisition and Attenuation Map Estimation for Multi-pinhole Clinical SPECT*. TU Delft; 2021.
6. Ivashchenko O, Have van der F, Villena JL, et al. Quarter-millimeter-resolution molecular mouse imaging with U-SPECT(+). *Mol Imaging*. 2014;13.
7. Nguyen MP, Ramakers RM, Kamphuis C, Koustoulidou S, Goorden MC, Beekman FJ. EXIRAD-3D: fast automated three-dimensional autoradiography. *Nucl Med Biol*. 2020;86–87:59-65.
8. Crawford JR, Robertson AKH, Yang H, et al. Evaluation of (209)At as a theranostic isotope for (209)At-radiopharmaceutical development using high-energy SPECT. *Phys Med Biol*. 2018;63(4):045025.
9. Huizing FJ, Hoeben BAW, Franssen GM, Boerman OC, Heskamp S, Bussink J. Quantitative imaging of the hypoxia-related marker CAIX in head and neck squamous cell carcinoma xenograft models. *Mol Pharm*. 2019;16(2):701-708.
10. Avram AM. Radioiodine scintigraphy with SPECT/CT: an important diagnostic tool for thyroid cancer staging and risk stratification. *J Nucl Med Technol*. 2014;42(3):170-180.
11. Delbeke D, Videlefsky S, Patton JA, et al. Rest myocardial perfusion/metabolism imaging using simultaneous dual-isotope acquisition SPECT with technetium-99m-MIBI/fluorine-18-FDG. *J Nucl Med*. 1995;36(11):2110-2119.
12. de Swart J, Chan HS, Goorden MC, et al. Utilizing high-energy gamma-photons for high-resolution 213Bi SPECT in mice. *J Nucl Med*. 2016;57(3):486-492.
13. Beekman FJ, Kamphuis C, Koustoulidou S, Ramakers RM, Goorden MC. Positron range-free and multi-isotope tomography of positron emitters. *Phys Med Biol*. 2021;66(6):065011.
14. Goorden MC, Beekman FJ. High-resolution tomography of positron emitters with clustered pinhole SPECT. *Phys Med Biol*. 2010;55(5):1265-1277.
15. Hwang AB, Iwata K, Hasegawa BH, Simulation of depth of interaction effects for pinhole SPECT. Nuclear Science Symp. Conf. Record IEEE, 2001. 3:1293-1297.
16. Korevaar MA, Heemskerk JW, Goorden MC, Beekman FJ. Multi-scale algorithm for improved scintillation detection in a CCD-based gamma camera. *Phys Med Biol*. 2009;54(4):831-842.
17. Korevaar MA, Heemskerk JW, Beekman FJ. A pinhole gamma camera with optical depth-of-interaction elimination. *Phys Med Biol*. 2009;54(13):N267-N272.
18. Nagarkar VV, Kudrolli H, Singh B. Focused scintillator array for high resolution gamma ray imaging. *IEEE Medical Imaging Conference*. 2010:M14-M98.
19. Alhassen F, Kudrolli H, Singh B, et al. Depth-of-Interaction compensation using a focused-cut scintillator for a pinhole gamma camera. *IEEE Trans Nucl Sci*. 2011;58(3):634-638.
20. Goorden MC, van der Have F, Kreuger R, et al. VECTor: a preclinical imaging system for simultaneous submillimeter SPECT and PET. *J Nucl Med*. 2013;54(2):306-312.
21. Beekman FJ, Focused pinhole gamma detection device. US Patent 8,067,741 B2. 2011.
22. Jan S, Santin G, Strul D, et al. GATE: a simulation toolkit for PET and SPECT. *Phys Med Biol*. 2004;49(19):4543-4561.
23. Hunter WCJ. *Modeling Stochastic Processes in Gamma-Ray Imaging Detectors and Evaluation of a Multi-Anode PMT Scintillation Camera for Use with Maximum-Likelihood Estimation Methods*. University of Arizona; 2007.
24. Haghshenas R, The effect of shape, size and arrangement of PMT'S on the intrinsic spatial resolution of anger camera, In 5th International and 17th National Iranian Congress of Nuclear Medicine. Shiraz Iran, 1-3 May, 2013.
25. Xia JS, Qian S, Wang W, et al. A performance evaluation system for photomultiplier tubes. *J Instrument*. 2015;10.
26. Jan S, Santin G, Strul D, et al. GATE: a simulation toolkit for PET and SPECT. *Phys Med Biol*. 2004;49(19):4543-4561.
27. NEMA. *Performance Measurements of Gamma Cameras*. *NEMA Standards Publication NU 1–2007*. National Electrical Manufacturers Association.
28. Barrett HH, Hunter WC, Miller BW, Moore SK, Chen Y, Furenlid LR. Maximum-likelihood methods for processing signals from gamma-ray detectors. *IEEE Trans Nucl Sci*. 2009;56(3):725.
29. Villena JL, Tapias G, Lage E, Kreuger R, Beekman FJ, Evaluation of a 25–511 keV list mode readout system for a large field-of-view gamma camera. 2010 IEEE Nuclear Science Symposium Conference Record (Nss/Mic), Knoxville, TN, 10 October–6 November 2010. IEEE; 2011. 2168-2173.

SUPPORTING INFORMATION

Additional supporting information can be found online in the Supporting Information section at the end of this article.

How to cite this article: Cosmi V, Wang B, Goorden MC, Beekman FJ. NaI gamma camera performance for high energies: Effects of crystal thickness, photomultiplier tube geometry and light guide thickness. *Med Phys*. 2024;1-13. https://doi.org/10.1002/mp.17043